electronics

MDPI

Article

A New Hybrid Sensor Design Based on a Patch Antenna with an Enhanced Sensitivity Using Frequency-Selective Surfaces (FSS) in the Microwave Region for Non-Invasive Glucose Concentration Level Monitoring

Umut Kose [1,2,*], Guliz Sili [1], Bora Doken [1], Emre Sedar Saygili [3], Funda Akleman [1] and Mesut Kartal [1]

[1] Department of Electronics and Communication Engineering, Istanbul Technical University, 34469 Istanbul, Turkey; dumangul@itu.edu.tr (G.S.); dokenb@itu.edu.tr (B.D.); akleman@itu.edu.tr (F.A.); kartalme@itu.edu.tr (M.K.)
[2] Department of Electrical and Electronics Engineering, Fatih Sultan Mehmet Vakif University, 34015 Istanbul, Turkey
[3] Division of Endocrinology and Metabolism, Department of Internal Medicine, Faculty of Medicine, Canakkale Onsekiz Mart University, 17100 Canakkale, Turkey; emre.saygili@comu.edu.tr
* Correspondence: ukose@fsm.edu.tr

Abstract

In this study, a hybrid sensor based on a defective square-truncated patch antenna (STPA) and a frequency-selective surface (FSS) was analyzed numerically and experimentally for different glucose–distilled water solutions. Here, an FSS was employed to enhance the sensitivity of the hybrid sensor. The sensing principle relies on monitoring variations in the loss tangent ($tan\delta$) and relative permittivity (ε_r) caused by different glucose concentrations applied to the sample under test (SUT). An open-ended coaxial probe was used to measure the complex permittivity of the solutions, which was then fitted to the Debye relaxation model. The simulated and experimental results of the novel sensor showed good agreement in a glucose concentration monitoring application. The sensor spanned the glucose range from 0 mg/dL to 5000 mg/dL, exhibiting a sensitivity of 55.44 kHz/mgdL^{-1} and a figure of merit (FOM) of 6.23 $\times$ 10^{-4} (1/mgdL^{-1}) in the experiments and 53.60 kHz/mgdL^{-1} and 1.71 $\times$ 10^{-4} (1/mgdL^{-1}) FOM in the simulations. When solutions with different concentrations were tested in the SUT, the resonance frequency of the antenna (f_0, in GHz) changed. To further characterize the sensor response, the relationship between the glucose concentration (C, in mg/dL) and f_0 was examined. A regression-based prediction model was constructed to map the measured scattering parameters to the glucose concentration, yielding a coefficient of determination (R^2) of 0.976. The high sensitivity, compact size, and compatibility with planar fabrication suggest that the proposed hybrid sensor has the potential to contribute to the development of non-invasive glucose-monitoring systems.

Keywords: hybrid biosensor; non-invasive sensor; microstrip antenna; frequency-selective surface (FSS); glucose level monitoring

Academic Editors: Zhen Liao, Jiayuan Lu and Xuanfeng Tong

Received: 1 January 2026
Revised: 14 January 2026
Accepted: 16 January 2026
Published: 19 January 2026

1. Introduction

Detecting, measuring, and analyzing things or situations using microwave signals is known as microwave sensing. While some advantages of microwave sensing include all-weather operation, non-contact measurements, and a high resolution, some challenges include interference, a limited penetration in conductive materials, and complex data

interpretation. Microwave sensing is a versatile and powerful technology for measuring critical parameters, including the concentration [1], flow rate [2], temperature [3,4], rotation [5], displacement [6], and humidity [1]. For example, metamaterial-based double-sided resonators were used to sense the humidity of chickpea powders and the concentration of methanol–deionized water solutions [1]. Usually, these measurements are made by tracking variations in the transmission, reflection, and absorption of microwave signals, which are affected by the sample of dielectric characteristics. The sensing method typically relies on detecting changes in the target environmental parameter, such as the pressure, temperature, humidity, or solution concentration, which in turn affects the dielectric constant of the sample under test (SUT). The resonance frequency and/or magnitude of the sensor structure vary with changes in the ambient parameter because it alters the relative permittivity and/or tangent loss [1].

The relationship between working at home and diabetes is a new research topic due to the adverse physiological effects brought about by remote working systems, accelerated globally by the COVID-19 pandemic. Although home office setups provide convenience and flexibility, they may also lead to lifestyle modifications that could impact the management of pre-existing diabetes or increase the risk of type 2 diabetes mellitus. Elevated blood glucose levels brought on by insufficient insulin synthesis, compromised insulin action, or both are hallmarks of diabetes mellitus [7,8]. Obesity, a decline in physical activity, and changing lifestyles are all prevalent variables that can lead to the development of this illness. If a diabetic patient's blood glucose levels change abruptly, appropriate treatment should be initiated immediately.

Glucose measurement methods used in devices that measure blood glucose levels are divided into three categories: invasive, minimally invasive, and non-invasive. In invasive glucose measurement, patients use a lancet to puncture their fingertips to obtain the necessary blood sample [7–12]. This procedure is complicated for patients with diabetes, particularly children, who must continuously check their blood glucose levels throughout the day. This approach is also financially infeasible due to the cost of disposable lancets and fixation tape. Furthermore, recurrent skin punctures can leave scars, even in small regions, increasing the risk of infection [7–12]. The drawbacks of intrusive techniques have made the development of novel detection techniques a popular area of study. In this context, non-invasive and minimally invasive techniques have received considerable attention recently. To measure blood glucose using an enzymatic approach, the minimally invasive method requires the collection of bodily fluids, such as perspiration, saliva, tears, etc. [7,8,11]. No bodily fluids are required for the non-invasive technique, which is based only on electromagnetic wave-material interaction [8,10,11,13–17].

Many glucose sensor types have been reported using various techniques, such as gas chromatography [18], high-performance liquid chromatography [19], spectrophotometry [20], optics [21], electrochemistry [22], and microwaves [23]. Electrochemical biosensors are the most extensively used due to their incredible accuracy and low cost. However, due to surface effects, these sensors exhibit significant response times. Similar to this, optical sensors respond very well to glucose, showing sharper peaks, less overlap, and resistance to fluorescence and luminescence interference [24]. However, this spectroscopy technique is more sensitive to changes in tissue thickness and density and requires longer stabilization times. Researchers have recently focused considerable attention on microwave biosensors due to their high readout speed, sensitivity, and reliability [25–27]. Because electromagnetic waves can penetrate the body, are highly sensitive, and are inexpensive to generate, microwave detection technologies are considered suitable for non-invasive measurement procedures [7,8,12]. Microwave sensing, widely applied across various fields, enables the detection of the glucose concentration in the body by leveraging tissue

and blood properties, such as reflection, transmission, and absorption, at these frequencies [7,8,12]. Components such as coplanar waveguides [28–30], resonators [9,11,25,31], and antennas [7–10,13,17,23,32,33], which are commonly used in the microwave region, are frequently employed in non-invasive glucose sensor applications.

Because of their low cost, passive operation, multimodal sensing, low design complexity, ease of integration with other devices, and ease of use, antenna-based sensors have become a promising alternative for non-invasive glucose detection in recent years [7,8,10,13,14,34]. Depending on changes in the detected material, the operating principles of antenna-based sensors often rely on variations in the resonance frequency of the antenna or amplitude at the resonance frequency [7,10,34]. In particular, by examining changes in the resonant frequency and amplitude of an antenna, one can identify the unique permittivity and conductivity properties of glucose molecules in the microwave and radio-frequency (RF) bands. This method provides a quick and painless way to monitor blood sugar levels without requiring blood extraction. Advances in materials science and microwave engineering have facilitated the development of antenna-based glucose sensors. For example, owing to their small size, affordability, and ease of integration into wearable technology, patch antennas and planar resonators have been extensively studied. Furthermore, the development of sensors that can adapt to the human body, thereby improving comfort and usability, has been enabled by biocompatible materials and flexible substrates. The potential uses of these sensors have been further expanded by recent research demonstrating that they can detect glucose levels in various biological fluids, including perspiration, saliva, and interstitial fluid. Despite these developments, several obstacles remain before antenna-based glucose sensors can be widely used. The accuracy of glucose measurements can be significantly impacted by interference from other biological components, including proteins and electrolytes [9]. Furthermore, environmental variables such as humidity and temperature might affect the sensor performance, requiring reliable calibration algorithms [9]. To mitigate these challenges, significant scholarly attention has been devoted to optimizing the sensing selectivity and operational reliability of these devices.

Metal arrays with a particular shape, regularly organized on a dielectric substrate, and designed to reflect, transmit, or absorb electromagnetic waves at specific frequencies are known as frequency-selective surfaces (FSSs) [8,35,36]. Applications of FSSs span several regions of the electromagnetic spectrum, including reflectors, absorbers, filters, lens antennas, antenna radomes, and sensors [8,35,36]. Researchers have typically employed FSSs as reflecting elements to increase the efficiency, gain, and bandwidth of antennas, as reported in the literature on combining antennas and FSSs into a hybrid [37]. In addition to these investigations, FSSs have recently been applied to enhance sensor sensitivity [7,8] and to match antenna impedance [35].

In this paper, we propose and experimentally validate a hybrid microwave sensor that integrates a frequency-selective surface (FSS) with a square-truncated patch antenna (STPA). The ground plane of the STPA was defected using an FSS comprising a 6×3 ring resonator (RR) unit cell. A properly defected ground plane allows for a reduction in the physical size of the antenna for its operating frequency and enables the creation of a more compact antenna structure. The FSS, another element of the sensor, consisted of a 6×3 RR unit cell. The SUT was located between the FSS and the antenna ground plane and was used to test samples with varying concentrations. Our motivation for the proposed sensor design was to enhance the sensitivity by increasing the coupling between the deformed ground plane and the FSS. This hybrid sensor structure was designed, fabricated, and tested for physical concentration sensing in glucose–distilled water solutions. Glucose–distilled water solutions prepared at different concentrations have different dielectric constant (ε_r)

and loss tangent ($tan\delta$) values. The sensing mechanism in this study was based on changes in the resonant frequency of the antenna due to variations in the solution concentration in the SUT region. The primary contributions of this study are summarized below:

- This work proposes a novel, low-cost, and simple technique for microwave region identification using a traditional antenna and an FSS.
- In this study, the FSS structure in the hybrid sensor structure was designed to increase the sensitivity rather than the antenna performance, as is customary.
- The relatively high sensitivity of the hybrid sensor structure compared to that reported in the literature, its compact size, and the thin and flexible nature of the base material used makes this sensor structure a strong alternative for wearable sensor applications.

The remainder of this paper is structured as follows: Section 2 provides a detailed description of the proposed hybrid sensor design, including the patch antenna and FSS geometry, as well as the numerical simulation setup. Section 3 presents the experimental methodology, detailing the preparation of glucose solutions and the measurement setup. In Section 4, the simulation and measurement results are presented and discussed, focusing on the sensor sensitivity, linearity, and performance metrics. Finally, Section 5 concludes the paper by summarizing the key findings and suggesting potential directions for future research.

2. Materials and Methods

2.1. Dielectric Properties of Glucose–Distilled Water Solution

In dielectric spectroscopy and materials science, the Cole–Cole and Debye models are frequently employed to explain the frequency-dependent behavior of dielectric materials [16,29,38,39]. The Cole–Cole model is used for more complex systems that exhibit relaxation-time dispersion, such as polymers, biological tissues, and glasses, whereas the Debye model is used for ideal systems with a single relaxation time, such as simple polar liquids. Although both models are used to describe relaxation processes in materials, their mathematical formulations and underlying assumptions differ. The complex permittivity of materials is frequently modeled using the Cole–Cole relaxation model (1).

$$\varepsilon^*(\omega) = \varepsilon^{'} - j\varepsilon^{''} = \varepsilon_\infty + \sum_n \frac{\Delta\varepsilon_n}{1 + (j\omega\tau_n)^{1-\alpha_n}} + \frac{\sigma_i}{j\omega\varepsilon_0} \tag{1}$$

In this equation, $\epsilon^{'}$ is the frequency-dependent permittivity, $\varepsilon^{''}$ is the frequency-dependent dielectric loss, ω is the angular frequency, ε_∞ is the high-frequency permittivity, n is the order of the Cole–Cole model, $\Delta\varepsilon_n$ is the magnitude of the dispersion, τ_n is the relaxation time constant, α_n is the variable that permits the dispersion to be widened, σ_i is the static ionic conductivity, and ε_0 is the permittivity of free space. The Debye model is the most widely used and straightforward model for describing dielectric relaxation. When $\alpha = 0$ and $\sigma_i = 0$, the Cole–Cole model reduces to the Debye model. For materials with a low conductivity, the section on static ionic conductance can be omitted [16,29,39]. It is also possible to model a glucose–distilled water solution in this manner. With the Debye parameters provided in (2)–(4) and the coefficients shown in Table 1, the permittivity can be computed in this range for any concentration value using (1). The coefficients used in (2)–(4), as given in Table 1, were appropriately determined to be consistent with the measurement results of the electrical properties of the solutions.

$$\varepsilon_\infty(\chi) = u_4 \times \chi^4 + u_3 \times \chi^3 + u_2 \times \chi^2 + u_1 \times \chi + u_0 \tag{2}$$

$$\Delta\varepsilon(\chi) = u_3 \times \chi^3 + u_2 \times \chi^2 + u_1 \times \chi + u_0 \tag{3}$$

$$\tau(\chi) = u_3 \times \chi^3 + u_2 \times \chi^2 + u_1 \times \chi + u_0 \quad (4)$$

Herein, χ represents the glucose concentration in mg/dL. The sensing approach employed in this study is based on measuring changes in the relative permittivity and loss tangent induced by various ratios of glucose–distilled water solutions placed in the SUT region. The eleven glucose–distilled water solutions that were tested in the SUT region were 0 mg/dL, 72 mg/dL, 216 mg/dL, 300 mg/dL, 500 mg/dL, 600 mg/dL, 1000 mg/dL, 1500 mg/dL, 3000 mg/dL, 4000 mg/dL, and 5000 mg/dL.

Table 1. Coefficients for the proposed Debye model parameters.

	u_4	u_3	u_2	u_1	u_0
$\varepsilon_\infty(\chi)$	2.0542×10^{-14}	-1.8774×10^{-10}	5.0497×10^{-7}	6.1540×10^{-6}	5.4444
$\Delta\varepsilon(\chi)$	–	-3.3059×10^{-11}	3.0253×10^{-7}	-1.4017×10^{-3}	74.0419
$\tau(\chi)$	–	7.7826×10^{-13}	-1.0155×10^{-9}	1.5363×10^{-4}	8.7785

2.2. Design and Fabrication of Hybrid Sensors

This study proposes a hybrid sensor with a square-truncated patch antenna (HSSTPA). Perspective schematic views of the HSSTPA and a photograph of the HSSTPA are shown in Figure 1a and Figure 1b, respectively. In Figure 1a, the interlayer is set to be transparent to better show both the antenna and the FSS layer. The interlayer was formed by placing a 14.4 mm × 2.4 mm × 29.7 mm sample under test (SUT) in a 15 mm × 3 mm × 30 mm sample holder. The sample holder was created on a 3D printer, a recently popular technology, using a polylactic acid (PLA) filament with a relative permittivity of 2.94 and a loss of 0.026 [40].

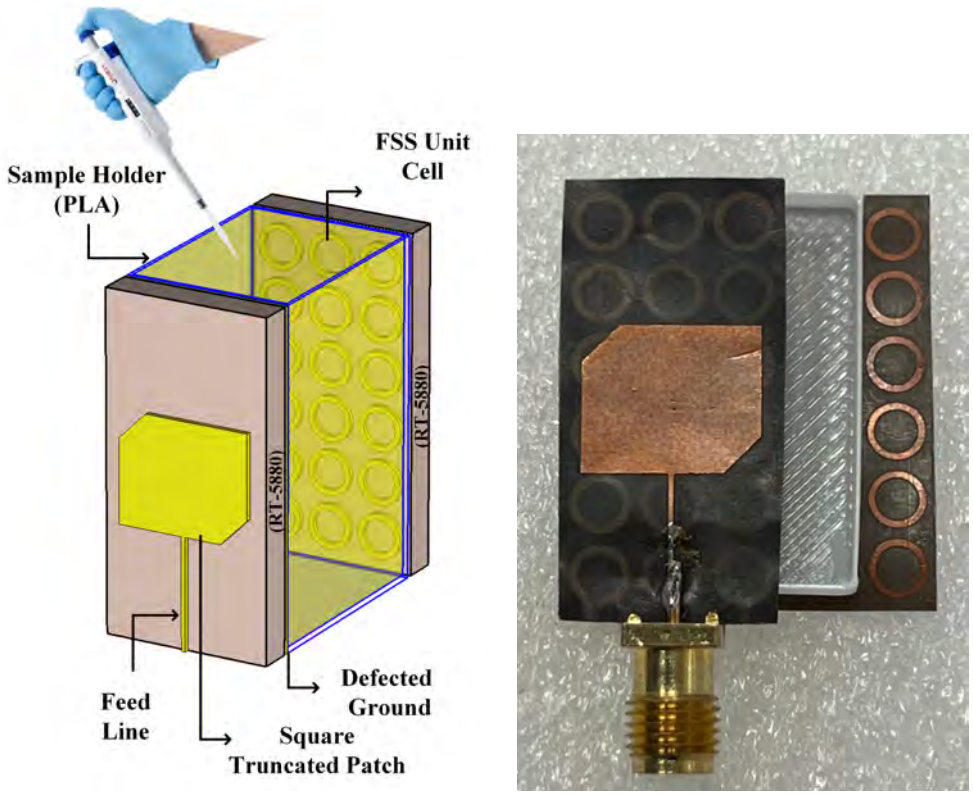

(**a**) (**b**)

Figure 1. (**a**) Perspective schematic view of the HSSTPA. (**b**) A photograph of the perspective view of the HSSTPA.

A schematic top view and the design parameters of the antenna section of the HSSTPA are shown in Figure 2a. Using the properties of the dielectric material, a 50 Ω microstrip transmission line fed the antenna in this instance. Since the main focus of the study was glucose level detection, no impedance-matching approaches were performed on the antennas; instead, only sensitivity augmentation was examined. Figure 2b shows a schematic bottom view and the design parameters of the antenna section of the HSSTPA. Herein, the ground plane of the STPA was defected using an FSS consisting of a 6 × 3 RR unit cell. The main purpose was to improve the sensitivity of the specified sensor by increasing the mutual coupling between the defected ground plane and the FSS. Figure 2c displays the design parameters and a schematic view of the FSS, another component of the hybrid sensor. Here, the FSS consisted of a 6 × 3 RR unit cell. Photographs of the top and bottom views of the antenna section of the manufactured sensor are shown in Figure 2d,e, while a photograph of the FSS section is shown in Figure 2f.

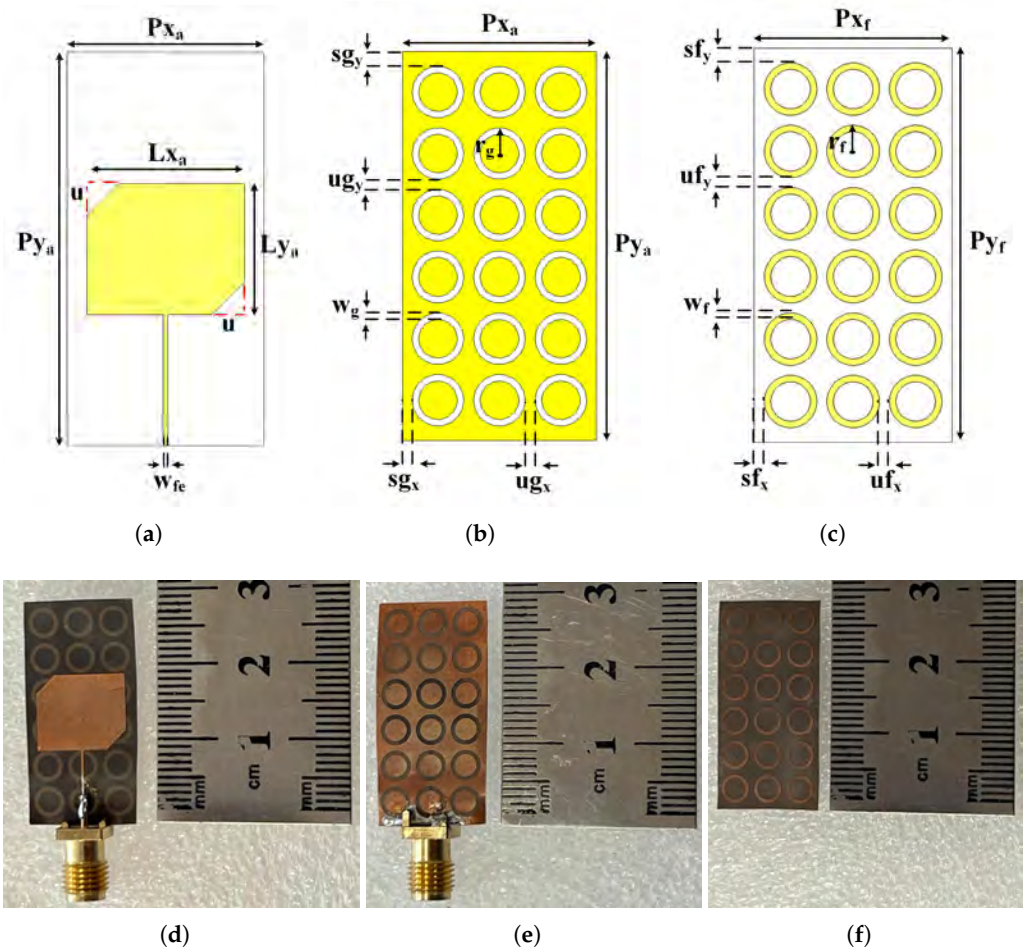

Figure 2. Schematic view and design parameters of the antenna section of the HSSTPA: (**a**) top and (**b**) bottom. (**c**) Schematic top view and design parameters of the FSS section of the HSSTPA. Photos of the antenna section of the HSSTPA: (**d**) top and (**e**) bottom. (**f**) A photo of the FSS section of the HSSTPA.

Table 2 lists the HSSTPA design characteristics and values in millimeters. An RT-5880 substrate with a relative permittivity of ε_{sub} = 2.2, a loss tangent $tan\delta_{sub}$ = 0.0009, a substrate thickness d_{sub} = 0.127 mm, and a metal (σ = 5.8 × 10 S⁄m) thickness t_m = 0.035 mm were used for all the sensor structures.

Table 2. The design parameters of the HSSTPA.

Parts of Hybrid Sensor	Antenna		Defected Ground of Antenna		FSS	
Design Parameters	Px_a	15.00	r_g	2.00	Px_f	15.00
	Py_a	30.00	w_g	0.50	Py_f	30.00
	Lx_a	12.00	sg_x	0.75	r_f	2.00
	Ly_a	10.00	sg_y	1.125	w_f	0.50
	w_{fe}	0.355	ug_x	0.75	sf_x	0.75
	u	4.50	ug_y	0.75	sf_y	1.125
	–	–	–	–	uf_x	0.75
	–	–	–	–	uf_y	0.75

3. Simulation and Experiment Setup

The method followed in this study consisted of the following steps: preparing different glucose–distilled water solutions, experimentally measuring the dielectric properties of these samples, using the obtained dielectric data in simulations within the CST Studio Suite® [41] under the frequency domain solver, and finally, performing the experimental characterization of the sensor using the PicoVNA 108 vector network analyzer. To prepare a series of glucose–water solutions with different concentrations, we mixed D-glucose monohydrate powder with distilled water. We prepared eleven sets of glucose solutions, with concentrations of 0 mg/dL, 72 mg/dL, 216 mg/dL, 300 mg/dL, 500 mg/dL, 600 mg/dL, 1000 mg/dL, 1500 mg/dL, 3000 mg/dL, 4000 mg/dL, and 5000 mg/dL, respectively. The complete dissolution of each solution was achieved using a magnetic stirrer, and all the samples were stored in sealed containers before the measurement. To minimize temperature-dependent changes in the dielectric properties, the ambient temperature was maintained at approximately 22.6 °C. Complex permittivity measurements of the prepared glucose–distilled water solutions used in the experiments were performed by using the Keysight (Agilent) N5230A PNA Series Network Analyzer and a commercial Speag DAK 3.5 mm diameter open-ended coaxial probe, as shown in Figure 3a. Open, short, and water calibration standards were used to calibrate the setup. The liquid to be measured was put in a glass beaker for the experiments, and the probe was submerged straight into the liquid. Isopropyl alcohol and a microfiber towel were used to clean the probe before measuring each liquid. The experimentally determined dielectric constant values were used directly as the material parameters in full-wave simulations performed on the three-dimensional electromagnetic model of the hybrid sensor. The 3D model of the sensor in the CST Studio Suite® [41] environment includes the illuminating antenna element, the dielectric substrate, the FSS structure, and the sensitive region containing the liquid sample. A waveguide port was used to excite the antennas during hybrid sensor simulations, and the computational domain was constrained by open-add walls. The SUT of the HSSTPA was defined separately for each glucose–water solution using the experimentally measured complex dielectric constant of the relevant sample; thus, a realistic prediction of the sensor's reflection coefficient ($|S_{11}|$) and shifts in the resonance frequency for different concentration levels was achieved. In the final stage, the experimental characterization of the produced hybrid sensor prototype was performed using a PicoVNA 108 vector network analyzer. The sensor was connected to the analyzer via a coaxial cable, and a single-port SOL (short–open–load) calibration was performed before starting the measurements to transfer the reference plane to the sensor input connector. For each glucose–water solution, a fixed volume (450 µL) of the sample was carefully loaded into a small-volume reservoir placed on the sensor's active region under a high electric field, with care taken to avoid

air bubbles. For each concentration, the $|S_{11}|$ was scanned to match the frequency range used in the simulations, and the average was evaluated based on multiple measurements. Resonance frequency values were extracted from the obtained reflection curves, and the frequency shifts calculated relative to pure water (0 mg/dL) were both compared with the simulation results and used as the input in the regression model for estimating the glucose concentration.

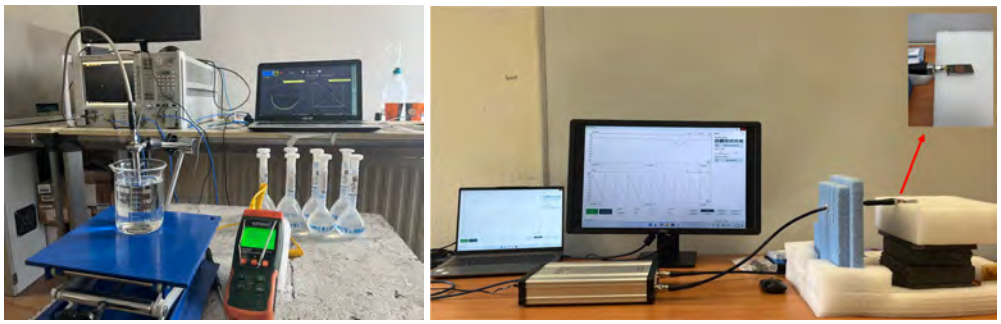

(**a**) (**b**)

Figure 3. Photos of experimental setup for (**a**) complex permittivity and (**b**) $|S_{11}|$ measurement.

4. Results

4.1. Dielectric Properties

Eleven different glucose–distilled water solutions were used to detect the glucose concentration. The frequency-dependent dielectric properties of the solutions, measured experimentally and calculated using the Debye model mentioned in Section 2, are shown in Table 3. For the 216 mg/dL solution, the real part of the complex permittivity is given in Figure 4a and the imaginary part of the complex permittivity is given in Figure 4b. For the detection performance analysis, the real and imaginary parts of each solution were treated as frequency distributions in the SUT region within the CST MWS environment.

Table 3. Electrical properties of glucose–distilled water solutions, measured and calculated using the Debye model.

Sample (mg/dL)	Freq. (GHz)	Debye Model		Measurement	
		ε'	ε''	ε'	ε''
0	6.010	72.156	22.114	72.074	22.092
72	6.050	71.964	22.225	71.864	22.303
216	6.060	71.758	22.212	71.829	22.339
300	6.090	71.597	22.323	71.687	22.461
500	6.140	71.292	22.458	71.388	22.517
600	6.150	71.188	22.484	71.226	22.778
1000	6.170	70.892	22.543	70.815	22.575
1500	6.200	70.617	22.657	70.616	22.801
3000	6.260	69.890	23.029	69.495	23.136
4000	6.270	69.327	23.224	69.200	23.373
5000	6.290	69.038	23.404	68.606	23.565

4.2. Simulation Results and Experimental Verification

In this study, an FSS was used to increase the sensitivity of the hybrid sensor. To demonstrate that the FSS increased the sensitivity in the proposed hybrid sensor structure, the FSS structure was removed from the hybrid sensor. This new sensor structure had the same dimensional parameters as the HSSTPA and is referred to as a sensor with a square-truncated patch antenna (SSTPA). The simulation and measurement results for the SSTPA

and HSSTPA are shown in Figure 5, using glucose–distilled water solutions prepared at different concentrations. As the solution concentration increased (from 0 mg/dL to 5000 mg/dL), a linear increase in the resonance frequency of the HSSTPA was observed. According to the simulation results in Figure 5, when the solution concentration increased from 0 mg/dL to 5000 mg/dL, an 84 MHz shift was observed in the SSTPA resonance frequency, while a 268 MHz shift was observed in the HSSTPA. As a result of the findings, a good agreement between the simulation and experimental results was observed.

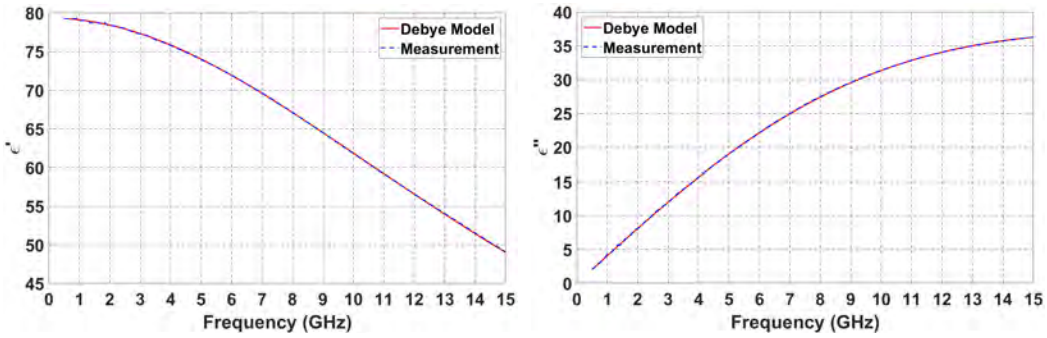

Figure 4. Measurement and calculation using the Debye model for a 216 mg/dL solution: (**a**) real part of complex permittivity (ε') and (**b**) imaginary part of complex permittivity (ε'').

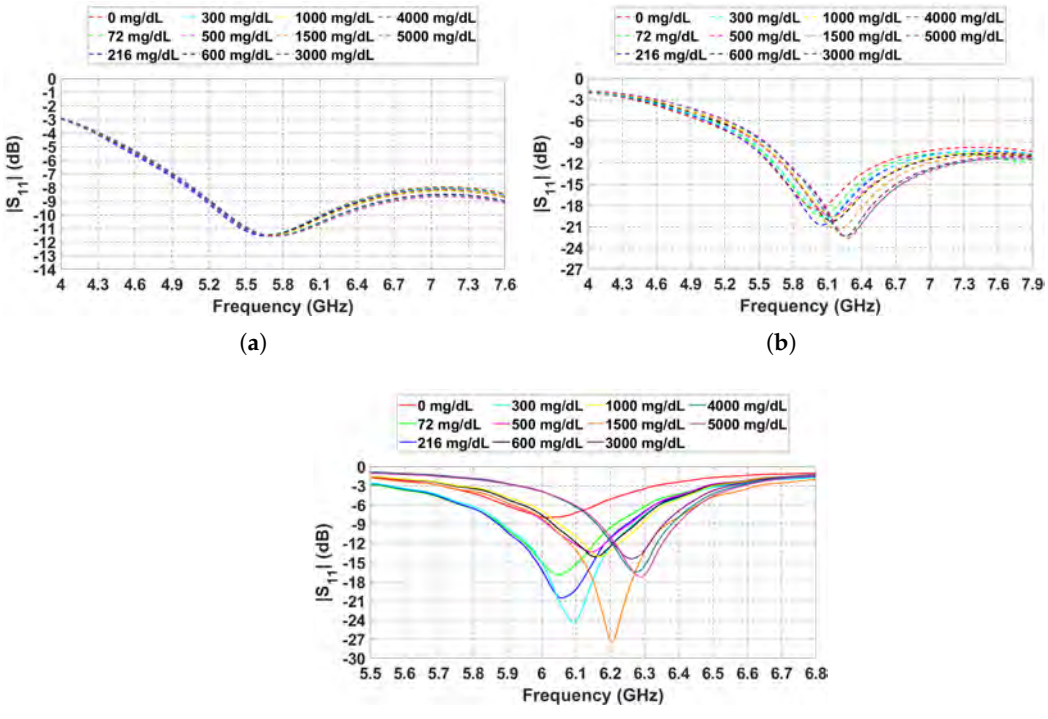

Figure 5. Frequency-dependent $|S_{11}|$ for different glucose–distilled water solutions. (**a**) SSTPA simulation, (**b**) HSSTPA simulation, and (**c**) HSSTPA experiment results.

The sensitivity (S) and figure of merit (FOM) are measures of success in sensor applications. The average sensitivity is the ratio of the absolute frequency shift (Δf) due to a change in the glucose–distilled water solutions (Δc) to the change in the glucose–distilled water solutions as given in (5) [7,8,10,18,31,32,42].

$$S = \Delta f / \Delta c \tag{5}$$

The resonance frequency (f_0) and $|S_{11}|$ at the resonant frequency are broken down in detail in Table 4. By successively adding the ε_r and $tan\delta$ values of several glucose–distilled water solutions in Table 3 to the SUT for the SSTPA and HSSTPA, the simulation and experiment produced these results. Table 4 shows a shift in the sensor's resonant frequency of 268 MHz and 277 MHZ in the simulation and experiments, respectively, for the suggested sensor construction (i.e., HSSTPA). On the other hand, the SSTPA simulation results showed a shift of 84 MHz in the resonant frequency. The sensitivity values calculated using (5) were determined to be 16.800 kHz/mgdL^{-1} for the simulation results of the SSTPA, 53.600 kHz/mgdL^{-1} for the simulation results of the HSSTPA, and 55.436 kHz/mgdL^{-1} for the measurement results of the HSSTPA.

Table 4. Simulation and experimental results obtained for HSSTPA and SSTPA tested using different solutions.

Sample (mg/dL)	SSTPA Sim.		HSSTPA Sim.		HSSTPA Meas.	
	f_0 (GHz)	$\|S_{11}\|$ (dB)	f_0 (GHz)	$\|S_{11}\|$ (dB)	f_0 (GHz)	$\|S_{11}\|$ (dB)
0	5.664	−11.540	6.008	−18.624	6.013	−7.997
72	5.664	−11.499	6.048	−19.564	6.050	−16.852
216	5.660	−11.546	6.052	−20.775	6.058	−20.544
300	5.672	−11.484	6.096	−19.818	6.091	−24.343
500	5.676	−11.489	6.136	−19.539	6.145	−13.382
600	5.688	−11.454	6.144	−20.181	6.155	−14.053
1000	5.700	−11.534	6.156	−19.552	6.170	−14.028
1500	5.700	−11.491	6.188	−21.517	6.205	−27.541
3000	5.724	−11.570	6.252	−22.403	6.262	−14.384
4000	5.732	−11.545	6.264	−22.312	6.273	−16.394
5000	5.748	−11.555	6.276	-22.615	6.290	−17.245
Δf_0, $\Delta\|S_{11}\|$ S (kHz/mgdL^{-1}), (dB/mgdL^{-1})	0.084 16.800	0.015 0.030	0.268 53.600	3.991 7.981	0.277 55.436	9.248 18.497

To evaluate the overall performance of the proposed structures, an FOM was calculated by integrating the quality factor (Q) values, excluding the sensitivity. Here, the FOM was calculated as the ratio of the sensitivity to the full width at half maximum (FWHM) [43]. The experimental results yielded a quality factor of 70.69, resulting in an FOM of 6.23 × 10^{-4} (1/mgdL^{-1}), while the simulation-based performance reached an FOM of 1.71 × 10^{-4} (1/mgdL^{-1}), with a quality factor of 20.06. In contrast, the SSTPA exhibited a quality factor of 3.153, yielding an FOM of 0.09 × 10^{-4} (1/mgdL^{-1}). This marked improvement in the FOM indicates that the HSSTPA structure provides a more robust balance between the sensing capability and the resonance sharpness, making it a more effective candidate for high-performance electronic sensing applications.

The numerically calculated electric-field distributions for the proposed sensors are illustrated in Figure 6 to evaluate the interaction between the resonator structures and the SUT. All subfigures use the same color scale (V/m) to enable direct and consistent comparisons. Figure 6a shows the SSTPA sensor with an empty SUT, representing the baseline field distribution. When a glucose–distilled water solution (216 mg/dL) was introduced into the SUT, a noticeable reduction in the overall field intensity was observed (Figure 6b), which can be attributed to the high permittivity and loss tangent of the aqueous solution absorbing a portion of the electromagnetic energy. A significant enhancement in the field concentration was achieved with the HSSTPA sensor, as shown in Figure 6c. The integration of the FSS layer effectively increased the electromagnetic coupling between the patch antenna and the FSS elements. This enhanced coupling led to a much denser and

more intense electric-field distribution within the SUT compared to the SSTPA design. The side-view profiles further confirmed that the HSSTPA sensor provided more uniform and deeper field penetration into the material, a critical factor for improving the sensitivity and detection accuracy in glucose-monitoring applications.

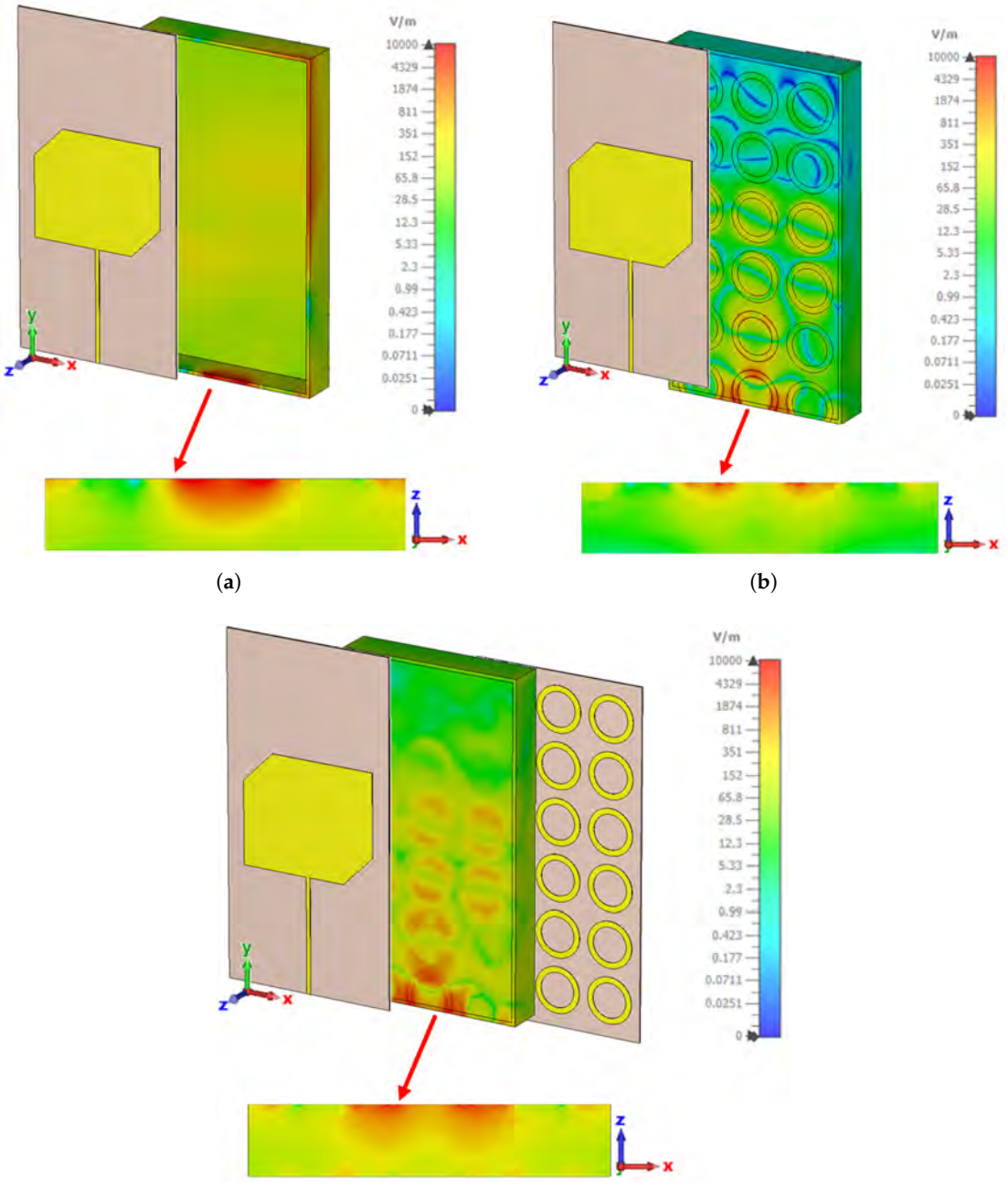

Figure 6. Numerically calculated electric-field distribution for the proposed sensors and the SUT: (**a**) SSTPA sensor with an empty SUT (no material inside); (**b**) SSTPA sensor with the SUT filled with a glucose–distilled water solution at 216 mg/dL; and (**c**) HSSTPA sensor with the SUT filled with a glucose–distilled water solution at 216 mg/dL. In each subfigure, the side view of the SUT and the corresponding electric-field distribution along the SUT are also shown.

Finally, a comparison table of sensor structures reported in the literature for the detection of glucose–distilled water solutions in the microwave region is presented in Table 5. The sensitivity of the proposed sensor was relatively higher than that of the sensor structures given in the articles referenced in [23,28–31], and it was lower

than or comparable to that of the sensor structures provided in the articles referenced in [17,25,32,33,42]. The HSSTPA had a more compact structure than all the articles presented in Table 5. In addition, the HSSTPA detected a wider concentration range (i.e., 0–5000 mg/dL), demonstrating that the sensor also works at high concentration values. Owing to its compact design and high sensitivity, the proposed sensor structure offers a promising approach to developing wearable, non-invasive glucose-monitoring systems.

Table 5. Cutting-edge methods for employing microwave sensors to measure glucose levels.

Ref.	Area (mm^2)	Freq. Range (GHz)	Sensor	Concentration (mg/dL)	Sensing Parameters	Substrate	Sensitivity (S) (kHz/(mg/dL))
[30]	22 × 12	4.46–4.48	coplanar waveguide	0–1800	$\|S_{11}\|$	RT-5880	3.88
[23]	N.A.	2.4–2.6	complementary split-ring resonator	5–80	$\|S_{11}\|$	RO-4350	5
[29]	34 × 16	3.4–3.6	microwave resonator integrated coplanar waveguide	0–2000	$\|S_{11}\|$	RO-3006	11
[28]	N.A.	0.6–0.8	interdigitated capacitor resonator-etched coplanar waveguide	0–8000	$\|S_{21}\|$	PET polyester	20
[31]	50 × 20	1.25–1.50	improved split-ring resonator	0–5000	$\|S_{21}\|$	RT-6006	26
[25]	42 × 40	1.8–2.5	differential microwave resonator with defected ground structure	0–360	$\|S_{21}\|$	N.A.	56.3
[42]	100 × 35	1.47–3.43	reconfigurable multi-mode sensing integrated with spoof surface plasmon polariton and spoof-localized surface plasmon	0–800	$\|S_{21}\|$	RO-4003	98.6
[33]	25 × 25	3.6–4.0	triple-ring microstrip patch antenna with defective ground structures	50–500	$\|S_{11}\|$	Teflon	245
[17]	55 × 55	4.0–4.5	hexagonal patch	50–250	$\|S_{11}\|$	RT-5880	352
[32]	35 × 35	2.25–2.5	monopole antenna	0–190	$\|S_{11}\|$	Textile	350
this work	30 × 15	6–6.4	HSSTPA	0–5000	$\|S_{11}\|$	RT-5880	55.4

4.3. Regression Model Performance

This section evaluates the performance of various regression models for describing the relationship between glucose–distilled water solutions (C, in mg/dL) and the corresponding resonance frequency (f_0, in GHz) of the proposed hybrid sensor. The objective was to obtain an accurate calibration curve that captures the observed nonlinearity across the entire solution range (0–5000 mg/dL). Initially, a linear regression model was applied to the experimental data. The resulting coefficient of determination was R^2 = 0.813. This indicates that a purely linear relationship is insufficient to fully represent the variation in the resonance frequency with glucose concentration, particularly at higher concentrations where a slight curvature was observed. To improve the fit, higher-order polynomial models were investigated. The second-order model equation is given in (6) and yielded R^2 = 0.940.

$$f(C) = -1.66 \times 10^{-8}C^2 + 1.27 \times 10^{-4}C + 6.0498 \quad (6)$$

This represents a substantial improvement over the linear model, indicating that a modest non-linearity in the relationship between the concentration and the resonance frequency is present and can be effectively captured by a second-order term. The third-order model equation is given in (7) and yielded R^2 = 0.976.

$$f(C) = 6.15 \times 10^{-12}C^3 - 6.15 \times 10^{-8}C^2 + 2.07 \times 10^{-4}C + 6.0304 \quad (7)$$

The third-order polynomial provided the best agreement with the experimental data, accounting for approximately 97.6 % of the variance in the resonance frequency. This model accurately fit the measured points across the entire concentration range and significantly reduced the residual error compared to both the linear and quadratic models. The measured data and the fitted third-order polynomial curve are shown in Figure 7a, where the close

agreement between the experimental and fitted values visually confirms the high quality of the regression model. Furthermore, to evaluate the performance over a more clinically relevant range, a detailed regression analysis was conducted for glucose concentrations between 0 mg/dL and 1000 mg/dL. This range encompasses the critical physiological and pathological glucose levels encountered in clinical diagnostics. As shown in Figure 7b, the third-degree polynomial model for this narrower range was calculated using (8), yielding an even higher coefficient of determination, $R^2 = 0.979$. This refined analysis enabled the clearer observation of intermediate values and demonstrates that the proposed hybrid sensor maintained an exceptional linearity and sensitivity in the most critical detection range, providing more precise calibration for practical healthcare applications.

$$f(C) = -2.6544 \times 10^{-10}C^3 + 2.2532 \times 10^{-7}C^2 + 1.9020 \times 10^{-4}C + 6.0203 \quad (8)$$

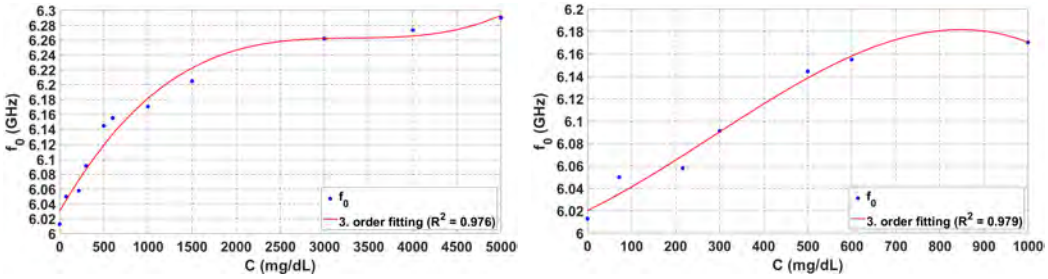

(**a**) (**b**)

Figure 7. Resonance frequency (f_0) versus glucose–distilled water solutions (C) graph for hybrid sensor: (**a**) 0–5000 mg/dL and (**b**) 0–1000 mg/dL.

5. Conclusions

This study presents a hybrid sensor that combines an STPA and an FSS for concentration sensing in glucose–distilled water solutions. Herein, an FSS was used to increase the sensitivity in a hybrid sensor structure, rather than for applications commonly used in the literature, such as increasing the efficiency, gain, and bandwidth of antennas and matching antenna impedance. Different glucose–distilled water solutions ranging from 0 mg/dL to 5000 mg/dL were tested in the SUT of the hybrid sensor. The resonance frequency of the hybrid sensor was analyzed as a function of the ε_r and $tan\delta$ values of the SUT, which offer a viable path toward reliable non-invasive glucose-monitoring systems. These values were then fitted to the Debye relaxation model. The simulated and experimental results correlate well in a glucose concentration monitoring application. According to experimental results, a sensitivity of 55.436 kHz/mgdL^{-1} was achieved for the tested concentration levels range. Measured scattering parameters were mapped to glucose concentration using a regression-based prediction model, which produced an R^2 of 0.976. The proposed hybrid sensor offers a viable path toward reliable non-invasive glucose-monitoring systems due to its high sensitivity, small size, and compatibility with planar manufacturing. The clinical implementation of the suggested hybrid sensor for continuous, non-invasive glucose monitoring will be the main focus of future research. The incorporation of biocompatible, flexible substrate materials will be investigated to achieve improved conformal contact with human skin, thereby improving the device's practical utility. To facilitate real-time data collection, a mobile application interface and a specialized signal-processing unit are also envisaged. To improve the overall robustness and dependability of the sensing platform, future research will also include extensive in vivo testing to assess the sensor's performance under various physiological conditions, including changes in body temperature, sweat composition, and multi-analyte interference.

Author Contributions: Conceptualization, U.K. and M.K.; methodology, U.K.; software, U.K.; validation, U.K. and G.S.; formal analysis, U.K.; data curation, U.K. and G.S.; writing—original draft preparation, U.K.; writing—review and editing, U.K., G.S., B.D., E.S.S., F.A., and M.K.; visualization, U.K.; supervision, M.K.; project administration, M.K. All authors have read and agreed to the published version of the manuscript.

Funding: This research was funded by the Scientific and Technological Research Council of Türkiye (TÜBİTAK), grant number 124E060. Available online: https://tubitak.gov.tr/tr (accessed on 1 January 2026).

Data Availability Statement: In this study, different glucose–distilled water solutions ranging from 0 mg/dL to 5000 mg/dL were prepared at 22.6 °C, and the electrical properties of these solutions were measured. Researchers can use these data from Table 3 in the article.

Conflicts of Interest: The authors declare no conflicts of interest. The funders had no role in the design of the study; in the collection, analyses, or interpretation of data; in the writing of the manuscript; or in the decision to publish the results.

Abbreviations

The following abbreviations are used in this manuscript:

STPA	Square-Truncated Patch Antenna
FSS	Frequency-Selective Surface
$tan\delta$	Loss Tangent
ε_r	Relative Permittivity
SUT	Sample Under Test
FOM	Figure of Merit
f_0	Resonance Frequency of the Antenna
C	Glucose Concentration
R^2	Coefficient of Determination
RF	Radio-Frequency
RR	Ring Resonator
HSSTPA	Hybrid Sensor with a Square-Truncated Patch Antenna
PLA	Polylactic Acid
SOL	Sort–Open–Load
$\|S_{11}\|$	Reflection Coefficient
ε'	Real Part of Complex Permittivity
ε''	Imaginary Part of Complex Permittivity
SSTPA	Sensor with a Square-Truncated Patch Antenna
S	Sensitivity
Δf	Absolute Frequency Shift
Δc	Change in Glucose–Distilled Water Solutions
Q	Quality Factor
FWHM	Full Width at Half Maximum

References

1. Ekmekci, E.; Kose, U.; Cinar, A.; Ertan, O.; Ekmekci, Z. The use of metamaterial type double-sided resonator structures in humidity and concentration sensing applications. *Sens. Actuators A Phys.* **2019**, *297*, 111559. [CrossRef]
2. Abduljabar, A.A.; Clark, N.; Lees, J.; Porch, A. Dual Mode Microwave Microfluidic Sensor for Temperature Variant Liquid Characterization. *IEEE Trans. Microw. Theory Tech.* **2017**, *65*, 2572–2582. [CrossRef]
3. Niksan, O.; Jain, M.C.; Shah, A.; Zarifi, M.H. A Nonintrusive Flow Rate Sensor Based on Microwave Split-Ring Resonators and Thermal Modulation. *IEEE Trans. Microw. Theory Tech.* **2022**, *70*, 1954–1963. [CrossRef]
4. Nath, U.; Banerjee, S.; Santini, C.; Citroni, R.; Mangini, F.; Frezza, F. Simple and Cost-Effective Design of a THz-Metamaterial-Based Hybrid Sensor on a Single Substrate. *Sensors* **2025**, *25*, 3660. [CrossRef] [PubMed]

5. Ebrahimi, A.; Withayachumnankul, W.; Al-Sarawi, S.F.; Abbott, D. Metamaterial-Inspired Rotation Sensor with Wide Dynamic Range. *IEEE Sens. J.* **2014**, *14*, 2609–2614. [CrossRef]
6. Wu, W.; Ren, M.; Pi, B.; Cai, W.; Xu, J. Displacement sensor based on plasmonic slot metamaterials. *Appl. Phys. Lett.* **2016**, *108*, 073106. [CrossRef]
7. Kose, U.; Kartal, M. A Low-Cost Microwave Hybrid Biosensor for Glucose Concentration Sensing. In *Proceedings of the 2024 International Conference on Applied and Theoretical Electricity (ICATE), Craiova, Romania, 24–26 October 2024*; IEEE: New York, NY, USA, 2024; pp. 1–5. [CrossRef]
8. Kose, U.; Kartal, M. Non-Invasive Microwave Glucose Sensor by Using a Hybrid Sensor Composed of a Frequency Selective Surface and Microstrip Patch Antenna. In *Proceedings of the 2023 Photonics & Electromagnetics Research Symposium (PIERS), Prague, Czech Republic, 3–6 July 2023*; IEEE: New York, NY, USA, 2023; pp. 1361–1367. [CrossRef]
9. Kandwal, A.; Sharma, Y.D.; Jasrotia, R.; Kit, C.C.; Lakshmaiya, N.; Sillanpää, M.; Liu, L.W.; Igbe, T.; Kumari, A.; Sharma, R.; et al. A comprehensive review on electromagnetic wave based non-invasive glucose monitoring in microwave frequencies. *Heliyon* **2024**, *10*, e37825. [CrossRef]
10. Raj, S.; Tripathi, S.; Upadhyay, G.; Tripathi, S.S.; Tripathi, V.S. An Electromagnetic Band Gap-Based Complementary Split Ring Resonator Loaded Patch Antenna for Glucose Level Measurement. *IEEE Sens. J.* **2021**, *21*, 22679–22687. [CrossRef]
11. Saleh, G.; Ateeq, I.S.; Al-Naib, I. Glucose Level Sensing Using Single Asymmetric Split Ring Resonator. *Sensors* **2021**, *21*, 2945. [CrossRef]
12. Villena Gonzales, W.; Mobashsher, A.; Abbosh, A. The Progress of Glucose Monitoring—A Review of Invasive to Minimally and Non-Invasive Techniques, Devices and Sensors. *Sensors* **2019**, *19*, 800. [CrossRef]
13. Mahnashi, Y.; Qureshi, K.K.; Al-Shehri, A.A.; Attia, H. Design and Experimental Validation of a Noninvasive Glucose Monitoring System Using RF Antenna-Based Biosensor. *IEEE Sens. J.* **2023**, *23*, 2856–2864. [CrossRef]
14. Harnsoongnoen, S. A Non-Contact Method for Detecting and Distinguishing Chloride and Carbonate Salts Based on Dielectric Properties Using a Microstrip Patch Sensor. *Chemosensors* **2023**, *11*, 158. [CrossRef]
15. Di Filippo, D.; Sunstrum, F.N.; Khan, J.U.; Welsh, A.W. Non-Invasive Glucose Sensing Technologies and Products: A Comprehensive Review for Researchers and Clinicians. *Sensors* **2023**, *23*, 9130. [CrossRef] [PubMed]
16. Yilmaz, T.; Foster, R.; Hao, Y. Radio-Frequency and Microwave Techniques for Non-Invasive Measurement of Blood Glucose Levels. *Diagnostics* **2019**, *9*, 6. [CrossRef]
17. Jeong, J.M.; Bien, F.; Lee, J.G. Design of Orientation-Independent Non-Invasive Glucose Sensor Based on Meta-Structured Antenna. *Electronics* **2025**, *14*, 2295. [CrossRef]
18. Xie, W.Q.; Gong, Y.X.; Yu, K.X. Rapid quantitative detection of glucose content in glucose injection by reaction headspace gas chromatography. *J. Chromatogr. A* **2017**, *1520*, 143–146. [CrossRef]
19. Armoogum, V.; Boodhoo, K. Full optimization and validation of an HPLC method for the quantitative analysis of total sugars in a soft drink. *Bull. Chem. Soc. Ethiop.* **2020**, *34*, 419–426. [CrossRef]
20. Bartosiak, M.; Giersz, J.; Jankowski, K. Analytical monitoring of selenium nanoparticles green synthesis using photochemical vapor generation coupled with MIP-OES and UV–Vis spectrophotometry. *Microchem. J.* **2019**, *145*, 1169–1175. [CrossRef]
21. Chang, J.H.; Lo, Y.L.; Cai, Z.Y.; Chang, C.M.; Wang, B.Y. Extraction of optical rotation angle in a turbid media using polarimetry system with single rotating polarizer. *Measurement* **2022**, *199*, 111508. [CrossRef]
22. Wu, H.; Yan, Y.; Huang, Q.; Liang, G.; Qiu, F.; Ye, Z.; Liu, D. A simple, cost-effective and selective analysis of glucose via electrochemical impedance sensing based on copper and nitrogen co-doped carbon quantum dots. *New J. Chem.* **2020**, *44*, 12723–12728. [CrossRef]
23. Ebrahimi, A.; Scott, J.; Ghorbani, K. Microwave reflective biosensor for glucose level detection in aqueous solutions. *Sens. Actuators A Phys.* **2020**, *301*, 111662. [CrossRef]
24. Lyandres, O.; Yuen, J.M.; Shah, N.C.; VanDuyne, R.P.; Walsh, J.T.; Glucksberg, M.R. Progress Toward an In Vivo Surface-Enhanced Raman Spectroscopy Glucose Sensor. *Diabetes Technol. Ther.* **2008**, *10*, 257–265. [CrossRef] [PubMed]
25. Xie, B.; Tang, X.; Wang, C.; Wu, Q. Integrated System for High-Sensitivity Differential Microwave Glucose Sensing. *IEEE Sens. J.* **2024**, *24*, 2975–2984. [CrossRef]
26. Juan, C.G.; Potelon, B.; Quendo, C.; Garcia-Martinez, H.; Avila-Navarro, E.; Bronchalo, E.; Sabater-Navarro, J.M. Study of Q_u-Based Resonant Microwave Sensors and Design of 3-D-Printed Devices Dedicated to Glucose Monitoring. *IEEE Trans. Instrum. Meas.* **2021**, *70*, 8005716. [CrossRef]
27. Dhakal, R.; Kim, E.; Jo, Y.H.; Kim, S.S.; Kim, N.Y. Characterization of micro-resonator based on enhanced metal insulator semiconductor capacitor for glucose recognition. *Med. Eng. Phys.* **2017**, *41*, 55–62. [CrossRef]
28. Tiwari, N.K.; Singh, S.P.; Mondal, D.; Akhtar, M.J. Flexible biomedical RF sensors to quantify the purity of medical grade glycerol and glucose concentrations. *Int. J. Microw. Wirel. Technol.* **2020**, *12*, 120–130. [CrossRef]
29. Turgul, V.; Kale, I. Permittivity extraction of glucose solutions through artificial neural networks and non-invasive microwave glucose sensing. *Sens. Actuators A Phys.* **2018**, *277*, 65–72. [CrossRef]

30. Yi, Z.; Wang, C. Noninvasive Glucose Sensors Using Defective-Ground-Structure Coplanar Waveguide. *IEEE Sens. J.* **2023**, *23*, 195–201. [CrossRef]
31. Govind, G.; Akhtar, M.J. Metamaterial-Inspired Microwave Microfluidic Sensor for Glucose Monitoring in Aqueous Solutions. *IEEE Sens. J.* **2019**, *19*, 11900–11907. [CrossRef]
32. Gharbi, M.E.; Fernández-García, R.; Gil, I. Textile Antenna-Sensor for In Vitro Diagnostics of Diabetes. *Electronics* **2021**, *10*, 1570. [CrossRef]
33. Zhang, M.; Yang, X.; Ren, M.; Mao, S.; Dhakal, R.; Kim, N.Y.; Li, Y.; Yao, Z. Microfluidic microwave biosensor based on biomimetic materials for the quantitative detection of glucose. *Sci. Rep.* **2022**, *12*, 15961. [CrossRef]
34. El Gharbi, M.; Fernández-García, R.; Ahyoud, S.; Gil, I. A review of flexiblewearable antenna sensors: Design, fabrication methods, and applications. *Materials* **2020**, *13*, 3781. [CrossRef] [PubMed]
35. Kose, U.; Kartal, M. Impedance Matching of Microstrip Patch Antennas by Using Frequency Selective Surfaces (FSS). In *Proceedings of the 2022 30th Signal Processing and Communications Applications Conference (SIU), Safranbolu, Turkey, 15–18 May 2022*; IEEE: New York, NY, USA, 2022; pp. 1–4. [CrossRef]
36. Anwar, R.; Mao, L.; Ning, H. Frequency Selective Surfaces: A Review. *Appl. Sci.* **2018**, *8*, 1689. [CrossRef]
37. Gangwar, D.; Das, S.; Yadava, R.L.; Kanaujia, B.K. Frequency Selective Surface as Superstrate on Wideband Dielectric Resonator Antenna for Circular Polarization and Gain Enhancement. *Wirel. Pers. Commun.* **2017**, *97*, 3149–3163. [CrossRef]
38. Cole, K.S.; Cole, R.H. Dispersion and absorption in dielectrics: II. Direct current characteristics. *J. Chem. Phys.* **1942**, *10*, 98–105. [CrossRef]
39. Karacolak, T.; Moreland, E.C.; Topsakal, E. Cole-cole model for glucose-dependent dielectric properties of blood plasma for continuous glucose monitoring. *Microw. Opt. Technol. Lett.* **2013**, *55*, 1160–1164. [CrossRef]
40. Cinar, A.; Basaran, S.C. 3D-printed sensor design based on metamaterial absorber for characterization of solid and liquid materials. *Sens. Actuators A Phys.* **2024**, *368*, 115166. [CrossRef]
41. *CST STUDIO SUITE®*, version 2025; Software for Electromagnetic Simulation; Dassault Systèmes, the 3DEXPERIENCE® Company: Darmstadt, Germany, 2025.
42. Wang, S.; Wang, W.; Zheng, Y. Reconfigurable Multimode Microwave Sensor with Resonance and Transmission Sensing Capabilities for Noninvasive Glucose Monitoring. *IEEE Trans. Microw. Theory Tech.* **2024**, *72*, 3102–3117. [CrossRef]
43. Cen, C.; Yi, Z.; Zhang, G.; Zhang, Y.; Liang, C.; Chen, X.; Tang, Y.; Ye, X.; Yi, Y.; Wang, J.; et al. Theoretical design of a triple-band perfect metamaterial absorber in the THz frequency range. *Results Phys.* **2019**, *14*, 102463. [CrossRef]